Journal of Photochemistry and Photobiology A: Chemistry 218 (2011) 143–155

Contents lists available at ScienceDirect

Journal of Photochemistry and Photobiology A: Chemistry

journal homepage: www.elsevier.com/locate/jphotochem

Formation, photophysics, and photochemistry of cadmium(II) complexes with 5,10,15,20-tetrakis(4-sulfonatophenyl)porphyrin and its octabromo derivative: The effects of bromination and the axial hydroxo ligand

Zsolt Valicsek[a], Ottó Horváth[a,*], György Lendvay[a,b], Ilijana Kikaš[c], Irena Škorić[c]

[a] Department of General and Inorganic Chemistry, Institute of Chemistry, Faculty of Engineering, University of Pannonia, P.O. Box 158, Veszprém H-8201, Hungary
[b] Institute of Structural Chemistry, Chemical Research Center, Hungarian Academy of Sciences, H-1525 Budapest, P.O. Box 17, Hungary
[c] Department of Organic Chemistry, Faculty of Chemical Engineering and Technology, University of Zagreb, Marulićev trg 19, 10000 Zagreb, Croatia

ARTICLE INFO

Article history:
Received 30 September 2010
Received in revised form
15 December 2010
Accepted 21 December 2010
Available online 28 December 2010

Keywords:
Water-soluble porphyrin
Out-of-plane
Cadmium(II) ion
Photochemistry
Bromination
Charge transfer

ABSTRACT

In slightly alkaline solution (pH 8) Cd(II) ion and 5,10,15,20-tetrakis(4-sulfonatophenyl)porphyrin (H_2P^{4-}) form a kinetically labile complex ($HOCdP^{5-}$), in which the metal center is located out of the ligand plane, due to the effects of the axial hydroxo ligand and the relatively large radius of Cd^{2+}. Both acidification and irradiation at the Soret-band can result in the dissociation of the axial ligand, reducing the out-of-plane distance of the metal center and the distortion of the macrocycle (CdP^{4-}). Besides, irradiation of both types of metalloporphyrins promotes an irreversible ligand-to-metal charge transfer leading to the oxidative degradation of the coordinated porphyrin at both the Soret- and the Q-bands. Under the same conditions, in the case of the octabromo derivative of this water-soluble porphyrin (H_2BrP^{4-}), the distorted structure accelerates the formation of the corresponding complex with cadmium(II) compared to its reaction with the parent, unbrominated ligand. The structure of this porphyrin ($HOCdBrP^{5-}$), similarly to the free base and $CdBrP^{4-}$ (formed via acidification of irradiation of $HOCdBrP^{5-}$), strongly distorted by the Br substituents significantly affects the characteristic features of the absorption and emission spectra, red-shifting the position of the main bands of these porphyrins compared to those of the unbrominated species. Also the emission quantum yields and lifetimes are dramatically diminished by bromination. Deviating from the unbrominated species, photodegradation of the brominated derivatives proved to be very oxygen sensitive. Besides, $CdBrP^{4-}$ is transformed into a new porphyrin derivative upon both Soret- and Q-band irradiation. DFT calculations of the geometrical structures and the absorption bands show good correlations with the observed photophysical and photochemical properties, due to the drastic distortions of the macrocyclic ligand.

1. Introduction

Metalloporphyrins represent one of the most significant families of compounds in biochemistry, due to their central role in photosynthesis, oxygen transport and biological redox processes [1–5]. Within this group the so-called out-of-plane (OOP) or sitting-atop (SAT) metalloporphyrins are characterized by special properties [6,7] originated from the nonplanar structure, for which, first of all, the size of the metal center is responsible. In these complexes, the metal, due to its large ionic radius (>80–90 pm), does not fit into the cavity of the ligand, hence it is located above the porphyrin plane, distorting it. The symmetry of this structure (generally $C_{4v} \rightarrow C_1$, originating from other structural effects) is lower than that of both the free-base porphyrin (D_{2h}) and the regular, coplanar metalloporphyrins (D_{4h}), in which the ionic radius of the metal center is smaller than 80–90 pm, fitting into the ligand cavity. The formation rate of metalloporphyrins is much slower for the in-plane or normal types than for the OOP complexes because of the inflexibility of porphyrins. In an OOP complex the distortion of the porphyrin caused by the out-of-plane location of the metal center makes two diagonal pyrrolic nitrogens more accessible on the other side of the ligand due to the increase of their sp^3 hybridization [8]. Thus, another metal ion, even with smaller ionic radius can easily coordinate to them. Hence, larger metal ions such as Pb^{2+}, Hg^{2+}, or Cd^{2+} can catalyse the formation of normal (in-plane) metalloporphyrins via generation of OOP complex intermediates [9–14]. Since the defor-

* Corresponding author at: Department of General and Inorganic Chemistry, Institute of Chemistry, University of Pannonia, Egyetem u. 10, H-8200 Veszprém, Hungary. Tel.: +36 88 624 159; fax: +36 88 624 548.
E-mail addresses: valicsek@vegic.uni-pannon.hu (Z. Valicsek), otto@vegic.uni-pannon.hu (O. Horváth), lendvay@chemres.hu (G. Lendvay), ilijana.kikas@gmail.com (I. Kikaš), iskoric@fkit.hr (I. Škorić).

1010-6030/$ – see front matter © 2010 Elsevier B.V. All rights reserved.
doi:10.1016/j.jphotochem.2010.12.014

mation of the porphyrin ring proved to be the main factor governing the acceleration of the metalloporphyrin formation [15,16], this can also be achieved by substituents at the porphyrin core or at the peripheral ring. Thus, e.g., the peripheral or β-substituted octabromoporphyrins display a buckled structure due to steric hindrance between the substituents [17–20]. Such a deformation profoundly enhanced the reactivity of the porphyrin even towards Hg^{2+} [21], the ionic radius of which is rather large anyway.

Although the literature regarding the spectroscopy, photophysics, and photochemistry of metalloporphyrins in non-aqueous media is abundant, however, considering that several properties of these complexes are generally characteristic to both hydrophobic and hydrophylic porphyrins, in the following, our survey is restricted largely to water-soluble porphyrin systems. Due to their special coordination and kinetic lability, SAT metalloporphyrins display peculiar photochemical features, such as photoinduced charge transfer from the porphyrin ligand to the metal center, finally leading to irreversible ring cleavage of the ligand, besides dissociation on excitation at both the Soret- and the Q-bands [22]. Moreover, the absorption and emission characteristics of these complexes are also significantly deviating from those of the normal (in-plane) metalloporphyrins. Since these properties are strongly influenced or determined by the structural distortion of these complexes, bromination of the porphyrin ligand, resulting in β-substituted octabromo derivative, may also significantly affect these features [23,24]. Besides, perhalogenation (e.g., octabromination) decreases the Lewis basicity of the porphyrin ligand, hence the coordinating ability of the metal center at the axial position can be enhanced towards another Lewis base such as HO^- [25].

While the photoinduced properties of normal metalloporphyrins have thoroughly been studied those of the OOP complexes were started to investigate only in the past 8–10 years. The size of cadmium(II) with ionic radius of 95 pm [26] is favourable for formation of OOP metalloporphyrins. Accordingly, there have been published several studies regarding the formation of such complexes of cadmium(II) with 5,10,15,20-tetrakis(4-sulfonatophenyl)-porphyrin [27–32]. The effect of bromination on this process was also examined, and it promoted the complex formation in the case of cadmium(II), while it was not favourable for Hg(II) with the same anionic porphyrin [29]. In spite of the numerous papers on the equilibrium of water-soluble porphyrin complexes of cadmium(II), photochemical features of these metalloporphyrins were hardly investigated. The light sensitivity of the cadmium(II) complex with this anionic porphyrin was only described in two articles focusing mainly on analytical applications [32,33].

On the basis of the precedents in this topic, the aim of our work, in the frame of a systematic investigation of the photophysics and photochemistry of water-soluble, sitting-atop metalloporphyrins, was to study the formation and mainly the photoinduced behaviour of the cadmium(II) complexes with 5,10,15,20-tetrakis(4-sulfonatophenyl)-porphyrin and its octabromo derivative (Fig. 1). For interpretation of the effects caused by the bromination theoretical calculations of the structures and absorption spectra were also carried out in this work.

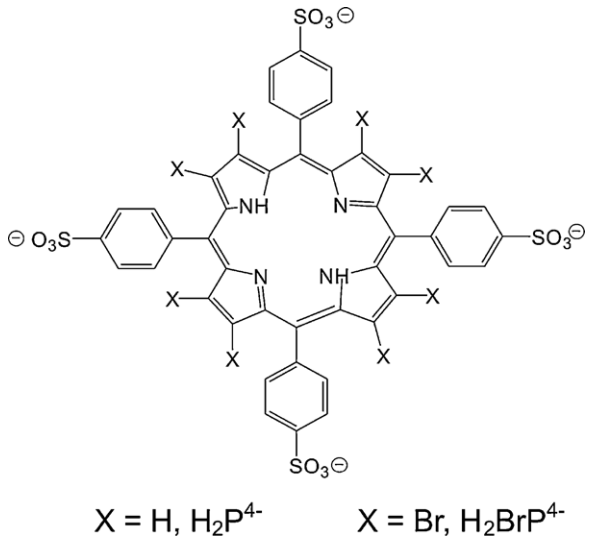

Fig. 1. Structures of 5,10,15,20-tetrakis(4-sulfonatophenyl)porphyrin, H_2P^{4-}, and its octabromo derivative, H_2BrP^{4-}.

2. Experimental

2.1. Synthesis of the brominated porphyrin

Preparation of 2,3,7,8,12,13,17,18-octabromo-5,10,15,20-tetrakis(4-sulfonatophenyl)-porphyrin was realized by a modified procedure of Tabata et al. [29]. In the first step tetraphenylporphyrin (H_2tpp) was brominated to form 2,3,7,8,12,13,17,18-octabromo-5,10,15,20-tetraphenylporphyrin (H_2obtpp). To a stirred solution of H_2tpp (0.5 g) in 35 cm^3 of dibromomethane *N*-bromosuccinimide (NBS, 1.5 g) was added. Stirring was continued at 100 °C for 2 days. After removal of the solvent the residue was purified by column chromatography on aluminium oxide using chloroform as eluent. The isolated product was characterized by UV–vis and ^{1}H NMR spectroscopy. The yield was 70%. The absorption maxima of H_2obtpp 1 were observed at 370, 468, 560, 621 and 733 nm in chloroform and ^{1}H NMR shifts at 8.21 (d, J = 6.9 Hz, 1H, o-H of phenyl), 7.82 (t, J = 7.3 Hz, 4H, p-H of phenyl), 7.77 (dd, J = 7.3; 6.9 Hz, 8H, m-H of phenyl) in $CDCl_3$. H_2obtpp was sulfonated in concentrated sulfuric acid at 90 °C for 8 h and then allowed to stand at room temperature for 2 days. Purification of the crude product was performed as follows: precipitation by careful addition of small amount of water, separation by centrifugation and washing with acetone to remove the remaining sulfuric acid and water. The product was further purified by column chromatography using basic alumina (Fluka) with water:methanol:acetone (7:2:1) as eluent. The final product, H_6obtpps (i.e., H_6BrP), was characterized by UV–vis and ^{1}H NMR spectroscopy. The UV–visible spectrum in aqueous solution displayed four peaks at 476, 596, 657, and 753 nm (details are given in Section 3.1). The ^{1}H NMR spectrum in D_2O showed two doublets due to protons on phenyl groups centered at 8.45 (d, J = 7.9 Hz, 8H, o-H) and 8.26 (d, J = 7.9 Hz, 8H, m-H).

2.2. Reagents and solutions

Beside the synthesized brominated porphyrin analytical grade tetrasodium 5,10,15,20-tetrakis(4-sulfonatophenyl)porphyrin (Na_4H_2tpps)·12H_2O and $CdCl_2$·2.5H_2O (Sigma–Aldrich) were used for the experiments. The reagents were dissolved in deionized, double-distilled water purified with Millipore Milli-Q system. Oxygen-free experiments were carried out by argon bubbling and Schlenk technique prior to the irradiation. The solutions containing metalloporphyrin were prepared well (at least 1 day) before the photophysical and photochemical experiments so that the complex equilibration was ensured. The actual concentrations of the porphyrin stock solutions prepared were checked spectrophotometrically, using the molar absorptions of the reagents at characteristic wavelengths. The pH of each solution was adjusted to 8 by application of borate buffer, also keeping the ionic strength at constant value of 0.01 M.

2.3. Instruments and procedures

The absorption spectra were recorded and the photometric titrations were monitored using a double-beam Perkin Elmer Lambda 25 and a Specord S-600 diode array spectrophotometer. For the measurement of fluorescence spectra a Perkin ELMER LS 50-B spectrofluorimeter was applied. The spectrum analyses were carried out by fitting Gaussian and Lorentzian curves in MS Excel. Rhodamine-B and $Ru(bpy)_3Cl_2$ were used as references for correction of the detector sensitivity and for determination of the fluorescence quantum yields [34,35]. Luminescence lifetime measurements were performed using a laser flash photolysis system previously described [36]. A Quantel Brilliant Nd:YAG laser yielding 355- and 532-nm pulses of about 5 ns duration served as a light source. The measurement data were recorded by a Tektronix DPO 4034 digital oscilloscope. Since the fluorescence lifetimes of the compounds studied are comparable with the laser half-width, a deconvolution method was applied for their determination [37].

For continuous irradiations an AMKO LTI photolysis equipment (containing a 200-W Xe–Hg-lamp and a monochromator) was applied [38]. Incident light intensity was determined with a thermopile calibrated by ferrioxalate actinometry [39,40]. Quartz cuvettes of 1 and 5 cm pathlength were utilized as reaction vessels. During the irradiations the reaction mixtures were continuously homogenized by magnetic stirring. All measurements were carried out at room-temperature. The experimental results were processed and evaluated by MS Excel programs on PCs.

2.4. Electronic structure calculations

Electronic structure calculations involved molecular geometry optimization and vibrational frequency analysis as well as the determination of vertical electron excitation energies. For both purposes we used density functional theory, in particular, the B3LYP combination of functionals [41–43], and time-dependent density functional theory. In the geometry optimizations we used the Hay–Wadt valence double-zeta (LANL2DZ) basis set [44–46] in which the influence of the inner-shell electrons on the valence shell is described using effective core potentials (ECP) for Cd and Br. This set, however, does not include polarization functions for the second-row elements of the periodic system. To check whether this causes any discrepancy, we re-optimized the structures by including polarization functions for these elements, using the LANLDZp set [47]. We found that the geometry change from the B3LYP/LANL2DZ optimum to LANL2DZp is less than 0.003 Å in bond lengths and 1° in bond angles. We note that the LANL2DZp basis set proved to be overcomplete in our molecules which caused serious SCF convergence problems. In the rest of the paper we present the results obtained at the LANL2DZ level. In the calculations we modeled H_2tpps^{4-} (H_2P^{4-}) and $H_2obtpps^{4-}$ (H_2BrP^{4-}) by H_2tpp and H_2obtpp, respectively. In our test calculations we found that the sulfonato substituent has a negligible effect on the coordination site.

All calculations were performed using the Gaussian 03 suite of programs [48]. The LANL2DZp basis set was downloaded from the EMSL Basis Set Exchange [49,50].

3. Results and discussion

3.1. Formation and absorption spectra

For examination of kinetically labile complexes mostly ligand excess is applied. However, in the case of metalloporphyrins, generally metal ions are used in excess, especially for spectrophotometric measurements, partly due to the extremely high molar absorbances (mainly at the Soret-bands) of the porphyrins. Deviating from the normal (in-plane) metalloporphyrins, the formation of kinetically labile SAT complexes is an equilibrium process. It can be followed spectrophotometrically because the absorption and emission bands assigned to ligand-centered electron transitions undergo significant shift and intensity change upon binding metal ions.

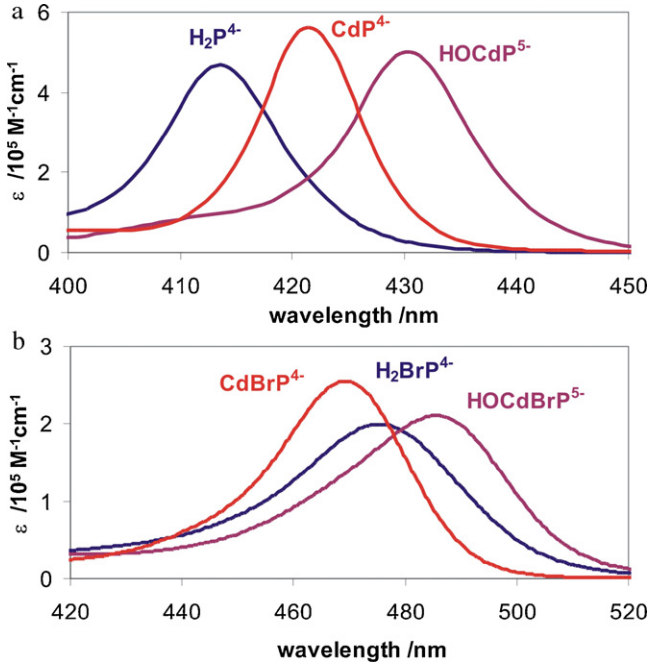

Fig. 2. Molar absorption spectra of H_2P^{4-} and its cadmium(II) complexes, CdP^{4-} and $HOCdP^{5-}$ (a), and those of the corresponding octabromo derivatives, H_2BrP^{4-}, $CdBrP^{4-}$, and $HOCdBrP^{5-}$ (b) at the Soret-band.

In aqueous solution cadmium(II) reacted easily with H_2P^{4-}, forming a complex with 1:1 composition at pH 8–12 [29,32,33,51]. The equilibrium constant for this reaction was also determined in several works [27–32] at different ionic strengths. At pH 8 (I = 0.01 M) we observed the formation of the 1:1 complex with the published characteristic Soret-band of 431 nm. Using the usual spectrophotometric titration method, we determined the equilibrium constant in this system ($\lg K'$ = 6.90) according to Eqs. (1) and (2) at adjusted pH of 8:

$$H_2P^{4-} + CdOH^+ \Leftrightarrow HOCdP^{5-} + 2H^+ \quad (1)$$

$$K = \frac{K'}{[H^+]^2} = \frac{[HOCdP^{5-}]}{[H_2P^{4-}][CdOH^+]} \quad (2)$$

This value is higher than those published earlier, mainly determined by pH titration (calculated from their data for pH 8: $\lg K'$ = 5.92 [27], 6.03 [28], 6.06 [29,30], 5.63 [31], 5.73 [32]). In most of the works dealing with the 1:1 complex, its composition was described as CdP^{4-}, without mentioning any axial ligand, except for Igarashi et al. [33], who indicated the coordination of a hydroxo ligand in axial position at pH is above 10. We found that the $HOCdP^{5-}$ complex is quantitatively formed at pH 8. Thus, the formation constants determined earlier in this system actually regard the latter compound (or a complex with two axial HO^- ligands at higher pH). In order to confirm this conclusion the solution of this complex was acidified to pH≈5. Under such a slightly acidic condition the axial HO^- ligand was removed, which was manifested in significant blue-shifts of the characteristic absorption bands (Fig. 2a and b). As it can be seen later in Section 3.3, irradiation can also promote the removal (dissociation) of the axial hydroxo ligand, leading to the CdP^{4-} species. Notably, this complex does not form directly in the

reaction of Cd^{2+} and H_2P^{4-} below pH 6, but its formation can be detected in the range of pH 7–8, suggesting that it is produced only through $HOCdP^{5-}$. Above pH 8, where the partial molar fraction of the aqua complex compared to the monohydroxo complex of cadmium(II) ion becomes essentially negligible, CdP^{4-} cannot form through $HOCdP^{5-}$ (further details of the formation kinetics will be published in a separate paper). This observation confirms the presence of the hydroxide ion in axial position on the cadmium(II) ion as central atom of the porphyrin complex. It is also important to note that CdP^{4-} and $CdBrP^{4-}$ formed by acidification at pH 5 or by photochemical reactions of $HOCdP^{5-}$ and $HOCdBrP^{5-}$ complexes, respectively, are stable at pH 8. Moreover, upon an increase in pH above 8 we have not observed a fast recovery of the original complexes, $HOCdP^{5-}$ and $HOCdBrP^{5-}$.

According to the literature, the octabrominated porphyrin (H_2BrP^{4-}) forms a complex with cadmium(II) even more readily than the unbrominated ligand does [29]. Formation of the complex with 1:1 composition could be spectrophotometrically followed in this system too, due to the strong red shifts of the characteristic absorption bands (Fig. 3). The equilibrium constant can only be estimated in our system ($\lg K' \approx 7.36$), but it is in good accordance with the data published earlier (calculated for our pH 8: $\lg K' = 7.40 \pm 0.13$ [29]). The formation rate constant ($\lg k_+(HOCdBrP^{5-}) = 4.82$) was ~19 times higher than that of the unbrominated complex ($\lg k_+(HOCdP^{5-}) = 3.55$). Similarly to the case of the unbrominated porphyrin, at pH 8 also this complex contains a hydroxo ligand in axial position ($HOCdBrP^{5-}$). In this case too moderate acidification (to pH ≈ 5) can remove it, leading to the formation of $CdBrP^{4-}$ (Fig. 3). The dissociation of this axial ligand also takes place upon photoexcitation as it will be shown in Section 3.3.

In Tables 1 and 2 are summarized the characteristic absorption data of the both the unbrominated species and their octabromo derivatives for the Soret- and Q-bands, respectively.

The band shifts refer to the Soret- or B(0,0) and the Q(0,0) transitions, where the first number in parentheses designates the vibrational quantum number of the excited (the S_2 and S_1 states, respectively), the second that of the ground electronic state [52,53]. The determination of the magnitude of the red shift is complicated because the presence of H atoms in free-base porphyrin reduces the symmetry ($D_{4h} \rightarrow D_{2h}$) and splits the Q-band ($Q \rightarrow Q_x + Q_y$) [54], therefore, there are generally five bands in this spectral region of free-base-, in contrast to three in those of metalloporphyrins [55] (Table 2). According to Gouterman's suggestion [56], the shift was calculated with respect to the average energy of $Q_x(0,0)$ and $Q_y(0,0)$ bands of free-base porphyrin.

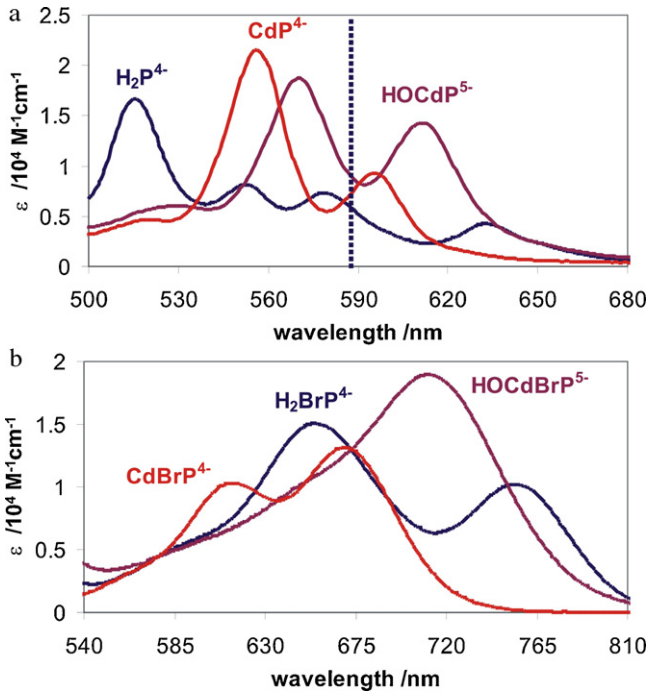

Fig. 3. Molar absorption spectra of H_2P^{4-} and its cadmium(II) complexes, CdP^{4-} and $HOCdP^{5-}$ (a), and those of the corresponding octabromo derivatives, H_2BrP^{4-}, $CdBrP^{4-}$, and $HOCdBrP^{5-}$ (b) at the Q-bands (the dotted vertical line represents the average of energy of $Q_y(0,0)$ and $Q_x(0,0)$ of free-base porphyrin). (For interpretation of the references to color in this figure legend, the reader is referred to the web version of the article.)

As a consequence of the coordination of cadmium(II) ion, both the Soret-bands (at 350–500 nm) and the Q-bands (at 500–700 nm) are red-shifted in the case of the unbrominated compounds. The molar absorbances of both the main Soret- and the Q-bands of the metalloporphyrins are higher than the corresponding values for the free-base porphyrin (Table 1). According to our earlier observations [22,57–61], this type of spectral properties is unambiguously characteristic for OOP or SAT complexes, confirming the expectations based on the size (95 pm ionic radius) of Cd(II).

The red shift of absorption in heavy-metal porphyrins can be attributed to that the metal orbitals are closer in energy to the antibonding π^* molecular orbitals (lowest unoccupied molecular orbitals, LUMOs) than to the binding π orbitals (highest occupied molecular orbital, HOMO) of porphyrin, so that the perturbation they cause decreases the energy of the LUMOs more than that of

Table 1
The Soret-absorption data of free-base and cadmium(II) porphyrins.[a]

Species	H_2P^{4-}	CdP^{4-}	$HOCdP^{5-}$	H_2BrP^{4-}	$CdBrP^{4-}$	$HOCdBrP^{5-}$
λ {B(1,0)}/nm	395	402	410	444	440	450
ε_{max} {B(1,0)}/10^4 M^{-1} cm^{-1}	8.09	5.63	8.60	3.63	5.97	5.76
λ_{Gauss} {B(1,0)}/nm	396	404	413	441	446	458
ε_{Gauss} {B(1,0)}/10^4 M^{-1} cm^{-1}	8.13	6.07	9.30	4.04	5.99	5.57
$\omega_{1/2}$ {B(1,0)}/cm^{-1}	1150	1270	1200	1680	1600	1480
f {B(1,0)}	0.36	0.30	0.43	0.26	0.37	0.32
ν {B(1,0)}/cm^{-1}	1090	1018	990	1655	1115	1228
λ {B(0,0)}/nm	413	421	431	476	470	486
ε_{max} {B(0,0)}/10^5 M^{-1} cm^{-1}	4.66	5.62	5.02	1.99	2.55	2.11
λ_{Gauss} {B(0,0)}/nm	414	422	431	475	470	485
ε_{Gauss} {B(0,0)}/10^5 M^{-1} cm^{-1}	4.45	5.37	4.67	1.91	2.36	1.96
$\omega_{1/2}$ {B(0,0)}/cm^{-1}	790	640	740	1520	1140	1290
f {B(0,0)}	1.35	1.32	1.34	1.12	1.04	0.98
B-shift (metalation)/cm^{-1}	–	−445	−943	–	244	−441
B-shift (bromination)/cm^{-1}	–	–	–	−3120	−2430	−2620

[a] λ, measured wavelength; λ_{Gauss}, wavelength from spectrum analysis; $\omega_{1/2}$, halfwidth; f, oscillator strength; ν, energy of vibronic overtone.

Table 2
Q-absorption data of free-base and cadmium(II) porphyrins (for notations see Table 1).

Species	H_2P^{4-} *y*	H_2P^{4-} *x*	CdP^{4-}	$HOCdP^{5-}$	H_2BrP^{4-}	$CdBrP^{4-}$	$HOCdBrP^{5-}$
λ {Q(2,0)}/nm	490		519	529	596	567	589
ε_{max} {Q(2,0)}/M^{-1} cm^{-1}	3350		4630	6020	5850	3494	5137
λ_{Gauss} {Q(2,0)}/nm	489		519	527	585	566	584
ε_{Gauss} {Q(2,0)}/M^{-1} cm^{-1}	3170		4910	6300	4500	2930	4440
$\omega_{1/2}$ {Q(2,0)}/cm^{-1}	1120		1340	1530	1930	1480	2010
f {Q(2,0)}	0.0137		0.026	0.037	0.034	0.0167	0.034
ν {Q(2,0)}/cm^{-1}	1080		1290	1440	1890	1360	1780
λ {Q(1,0)}/nm	516	579	556	570	657	615	651
ε_{max} {Q(1,0)}/M^{-1} cm^{-1}	16,660	6670	21,500	18,730	15,070	10,310	10,460
λ_{Gauss} {Q(1,0)}/nm	517	582	556	570	658	613	651
ε_{Gauss} {Q(1,0)}/M^{-1} cm^{-1}	16,060	6160	20,600	17,820	14,520	9800	8580
$\omega_{1/2}$ {Q(1,0)}/cm^{-1}	830	850	820	880	1730	1310	1770
f {Q(1,0)}	0.051	0.020	0.065	0.060	0.097	0.050	0.059
ν {Q(1,0)}/cm^{-1}	1180	1390	1180	1210	1960	1430	1390
λ {Q(0,0)}/nm	553	633	596	611	753	670	712
ε_{max} {Q(0,0)}/M^{-1} cm^{-1}	6990	3980	9240	14,280	10,180	13,150	18,960
λ_{Gauss} {Q(0,0)}/nm	550	633	595	612	755	672	716
ε_{Gauss} {Q(0,0)}/M^{-1} cm^{-1}	6430	3680	9050	13,710	9750	12,660	17,100
$\omega_{1/2}$ {Q(0,0)}/cm^{-1}	830	730	720	880	1050	1220	1460
f {Q(0,0)}	0.021	0.010	0.025	0.046	0.040	0.060	0.097
B–Q energy gap/cm^{-1}	7170		6910	6880	7800	6400	6640
Q-shift (metalation)/cm^{-1}	–	–	−184	−650	–	1640	720
Q-shift (bromination)/cm^{-1}	–	–	–	–	−3740	−1920	−2380
$\varepsilon(B_{max})/\varepsilon(Q_{max})$	28.0		26.2	26.8	13.2	19.4	11.1
f(B)/*f*(Q)	14.7		14.0	12.3	8.1	11.2	6.9

the HOMO, resulting in the bathochromic effect of $\pi\pi^*$ transitions. Besides, the structural change of the macrocyclic ligand, due to the interaction with the metal center of large ionic radius, may also contribute to this spectral feature. Not only metalation of the free base (H_2P^{4-}), but also axial coordination of, e.g., a hydroxo ligand to CdP^{4-} is accompanied by red shifts of the characteristic absorption bands. As the corresponding values indicate for B(0,0), the axial ligand causes a slightly larger red shift than the metalation itself (−498 cm^{-1} vs. −445 cm^{-1}, Table 1), according to the larger out-of-plane distance in the case of $HOCdP^{5-}$, resulting in the higher dome-distortion of the porphyrin ligand. For the Q(0,0)-band the effect of the axial ligand is much stronger (−184 cm^{-1} vs. −466 cm^{-1}, Table 2), indicating that the energy of the S_1 state is more influenced by this structural change. As a consequence of intensity borrowing, transitions to higher vibrational levels of the excited electronic states also appear in the spectra of porphyrins [62,63]. The frequencies of the vibronic overtones for the porphyrins studied in this work (ν in Tables 1 and 2) were determined by spectrum analysis (more accurately than taken directly from the measured spectra). The tendencies of the frequencies of the vibronic overtones obtained for H_2P^{4-}, CdP^{4-}, and $HOCdP^{5-}$ are the same as those observed for the main bands (B(0,0) and Q(0,0)). The energy gap between the B(0,0)- and Q(0,0)-bands is almost constant, about 7000 cm^{-1} [61]. This similarity may be explained by that the metalation and the axial ligand result in the same perturbation on the S_1- and S_2-states of the porphyrin ligand. This is also manifested in the similar values of $\varepsilon(B_{max})/\varepsilon(Q_{max})$ and *f*(B)/*f*(Q) ratios, respectively (Table 2).

In the case of the brominated porphyrins, both the Soret- and the Q-bands are significantly red-shifted compared to those of the corresponding unbrominated compounds (Fig. 3a and b, Tables 1 and 2). Such a phenomenon was observed for the first time for nonionic free-base and metalloporphyrins and attributed to configurational interactions [17,64]. This interpretation based on the Gouterman's four-orbital approach [65] could also be applied for water-soluble porphyrins and their metal complexes [66]. Nevertheless, the very strong distortion of the porphyrin ring caused by the sterically packed peripheral substituents may also contribute to this spectral effect. However, the split of the Q-bands is questionable in the brominated free-base porphyrin because only three Q-bands appear, in contrast to five as in the unbrominated ligand (Fig. 3 and Table 2). While metalation of the unbrominated free-base porphyrin leads to considerable bathochromic shifts of both the Soret- and the Q-bands, insertion of cadmium(II) into the cavity of the brominated free base results in significant hypsochromic shifts of these bands. This very unusual phenomenon in the case of the OOP complexes may be attributed to the decrease of the distortion of the macrocycle. Coordination of the axial hydroxo ligand may appreciably increase the distortion again, as the red shifts of the characteristic bands indicate (Tables 1 and 2). In the case of the Soret-bands the wavelengths for $HOCdBrP^{5-}$ are even longer than those for $CdBrP^{4-}$. The magnitude of the red shifts caused by the bromination are the largest for the B(0,0)- and Q(0,0)-bands of the free-base porphyrin, however, the large shift of the Q-band can partly originate from the lack of the above-mentioned split. In the case of the complex with axial hydroxo ligand the corresponding values are lower, while the lowest ones were observed for the metalloporphyrin without axial ligand, probably due to the least distorted structure. Generally, the molar absorbances and also the oscillator strengths of the Soret-bands (B(0,0)) are significantly lower for the brominated derivatives compared to those of the unbrominated species. (The only exception is the B(1,0)-band for $CdBrP^{4-}$.) In the case of the Q-bands, however, the corresponding values for the free base are higher for the brominated derivatives. For the metalloporphyrins, the Q(2,0)- and Q(1,0)-bands are weaker, while the Q(0,0)-bands are stronger than the corresponding ones for the unbrominated species. This phenomenon suggests that the bromination more considerably affects the transition to the S_2-state than to the S_1-state. Accordingly, the values of $\varepsilon(B_{max})/\varepsilon(Q_{max})$ and *f*(B)/*f*(Q) ratios are significantly lower than those for the unbrominated species, especially for $HOCdBrP^{5-}$.

3.2. Emission

The fluorescence spectra of H_2P^{4-}, CdP^{4-}, and $HOCdP^{5-}$ are compared in Fig. 4a. The characteristic data for the fluorescence of the unbrominated species and the brominated derivatives are summarized in Tables 3 and 4, respectively. In the case of the unbrominated species the analysis of the spectra reveals the hitherto unknown Q(0,2) fluorescence band, which is the counterpart

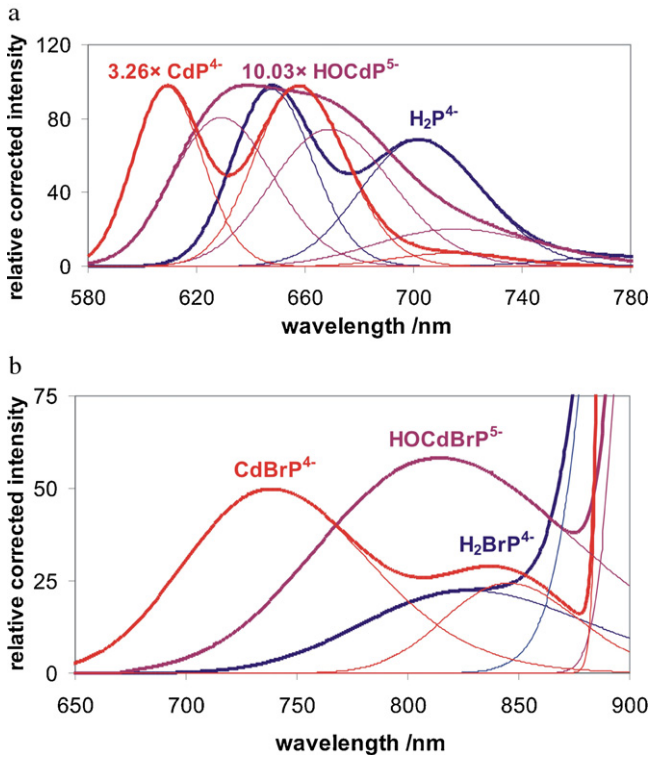

Fig. 4. The analysed fluorescence spectra of H_2P^{4-} and its cadmium(II) complexes, CdP^{4-} and $HOCdP^{5-}$ (a), and those of the corresponding octabromo derivatives, H_2BrP^{4-}, $CdBrP^{4-}$, and $HOCdBrP^{5-}$ (b).

of the Q(2,0) absorption band. Metalation of the porphyrin results in a hypsochromic effect in the fluorescence: the (0,0) band is shifted by almost 1000 cm^{-1} (Table 3), in contrast to the red shift in the absorption. Notably, this blue shift–red shift anomaly is virtual, because the absorption shift is referred to the average of $Q_y(0,0)$- and $Q_x(0,0)$-bands of the free-base ligand, while the emission derives not from a hypothetical average level, but from the energetically lower S_{1x}-state (populated in $Q_x(0,0)$ absorption). Coordination of the axial hydroxo ligand considerably decreases the value of the S_1-shift, to less than half of that for CdP^{4-}, indicating a diminished interaction between the porphyrin and the metal center. The shift of the Q(0,0) transition ($Q_x(0,0)$ in the case of H_2P^{4-}) between absorption and emission, i.e., the S_1 Stokes-shift characterises the magnitude of the structural change during excitation. The Stokes-shift is a bit larger in CdP^{4-} than in H_2P^{4-}, although the complex is slightly nonplanar already in the ground state, while the free base is quite planar. This observation gives some information about the excited-state geometry. For this it is important that monoporphyrin complexes of numerous different metal ions were found to have very similar vibronic overtones (ν_1 is about 1200 cm^{-1} almost independently of the nature of the metal ion) [61], thus in the S_1-excited-state these metalloporphyrins can be assumed to have the same degree of ring deformation. On the basis of this assumption, from the relatively large Stokes-shift for CdP^{4-} one can conclude that in the ground state, although it is not quite planar, this complex is farther from the assumed "common" excited-state geometry. The latter structure is possibly even more nonplanar based on the observation that thallium(III) porphyrin, which in the ground state is farther from being planar than CdP^{4-}, has a smaller Stokes-shift (242 cm^{-1}) [60], while the corresponding complex of mercury(II) having larger ionic radius (102 pm) than Tl(III) (88 pm) has a larger Stokes-shift (400 cm^{-1}) [61], similar to CdP^{4-}. Coordination of the axial hydroxo ligand significantly increases the Stokes-shift, indicating a more nonplanar distortion in the S_1-excited state compared to that of the ground state.

As seen in Table 3, coordination of cadmium(II) ion to the unbrominated porphyrin significantly decreases both the estimated quantum yield and lifetime of S_1-fluorescence, by a factor of about 3 for each parameter. According to our measurement, the lifetime of the unbrominated free base is 10 ns [61], which is similar to the published data for H_2tpp: τ_{S1} = 16 [67], 13.6 [68], 10.4 [53], and 12.4 ns [69].

Although no literature value is available for the lifetime of fluorescence of CdP^{4-}, τ_{S1} (3.4 ns) which we obtained is similar to those of other out-of-plane porphyrins with Soret absorption maximum at 421 nm [61,70]. It is known that the efficiency of nonradiative decay increases with the deformation, especially with the out-of-plane position of metal center [71] and, accordingly, that also the yield of fluorescence decreases if the symmetry of a structure is reduced [72]. The values of the rate constants of the radiative and nonradiative processes calculated from the corresponding data for H_2P^{4-} and CdP^{4-}, along with the quantum yields indicate that this is the case in this system, too. Upon the coordination of Cd^{2+} to the porphyrin, k_{nr} increases by a factor of 3, while k_r is nearly constant. This suggests that in this case the acceleration of nonradiative decay is responsible for the reduction of the fluorescence lifetime and not the deceleration of the radiative process. The observation that

Table 3
The S_1-fluorescence data of CdP^{4-} and $HOCdP^{5-}$, compared with those of H_2P^{4-}.[a]

Species	H_2P^{4-}			CdP^{4-}			$HOCdP^{5-}$		
transition	$S_1(0,0)$	$S_1(0,1)$	$S_1(0,2)$	$S_1(0,0)$	$S_1(0,1)$	$S_1(0,2)$	$S_1(0,0)$	$S_1(0,1)$	$S_1(0,2)$
λ {$S_1(0,i)$}/nm	648	702	775	609	658	714	629	669	716
$I_{max}(0,i)/I_{max}(0,0)$	–	0.712	0.0527	–	1.000	0.0721	–	0.920	0.250
$\omega_{1/2}$ {$S_1(0,i)$}/cm^{-1}	830	1070	1010	810	920	990	1100	1180	1390
ϕ {$S_1(0,i)$}	0.038	0.035	0.0024	0.012	0.013	0.0010	0.0045	0.0044	0.0014
ν {$S_1(0,i)$}/cm^{-1}	–	1200	1340	–	1210	1190	–	950	970
S_1-shift (metalation)/cm^{-1}		–			980			450	
S_1-Stokes/cm^{-1}		360			390			450	
$\phi(S_1)$		0.075 (0.062[b])			0.026			0.010	
$\Phi(S_1–B)$		0.056			0.022			0.0027	
ϕ(IC)		0.75 (0.83[b])			0.83			0.27	
$\tau(S_1)$/ns		10.0			3.4			0.36 (0.26[c])	
$k_r(S_1)/10^6$ s^{-1}		7.5			7.6			28.8	
$k_{nr}(S_1)/10^7$ s^{-1}		9.2			28.6			279	
k_r(Strickler–Berg)/10^6 s^{-1}		8.2			33.7			39.5	

[a] $\Phi(S_1–B) = \varphi(IC\ S_2 \rightarrow S_1) \times \varphi(S_1)$ and $k_r(S_1) = \varphi(S_1)/\tau(S_1)$.
[b] From Q_y-state.
[c] Estimated by the Strickler–Berg-equation.

Table 4
The S_1-fluorescence data of $CdBrP^{4-}$ and $HOCdBrP^{5-}$, compared with those of H_2BrP^{4-} (for notations see Table 3).

Species	H_2BrP^{4-}		$CdBrP^{4-}$		$HOCdBrP^{5-}$	
transition	$S_1(0,0)$	$S_1(0,1)$	$S_1(0,0)$	$S_1(0,1)$	$S_1(0,0)$	$S_1(0,1)$
λ {$S_1(0,i)$}/nm	828	972	739	845	815	905
$\omega_{1/2}$ {$S_1(0,i)$}/cm^{-1}	1740	980	1790	990	2050	300
ϕ {$S_1(0,i)$}	3.7×10^{-5}	2.6×10^{-3}	1.2×10^{-3}	3.2×10^{-4}	7.5×10^{-3}	2.7×10^{-3}
ν {$S_1(0,i)$}/cm^{-1}	–	1790	–	1710	–	1220
S_1-shift (metalation)/cm^{-1}	–		1460		199	
S_1-shift (bromination)/cm^{-1}	−3360		−2880		−3620	
S_1-Stokes/cm^{-1}	1170		1350		1690	
$\phi(S_1)$	2.7×10^{-3}		1.5×10^{-3}		1.0×10^{-2}	
$\Phi(S_1\text{–B})$	4.4×10^{-4}		3.9×10^{-4}		1.1×10^{-3}	
ϕ(IC)	0.17		0.27		0.10	
$\tau(S_1)$/ns	0.15[a]		0.062[a]		0.35[a]	
k_r(Strickler–Berg)/10^6 s^{-1}	17		25		29	

[a] Estimated by the Strickler–Berg-equation.

the fluorescence lifetimes are hardly affected by the nature of the metal center implies that probably the geometry is the determining factor in the balance of excited-state processes. Coordination of the axial hydroxo ligand dramatically decreases both the quantum yield and the lifetime of the fluorescence. Since the lifetime in this case is about one order of magnitude shorter than that of the pulse duration in our laser system, it could be only roughly estimated by deconvolution (0.36 ns), however, this estimation is in a good accordance with the value predicted by the Strickler–Berg equation [73] (0.26 ns). As the corresponding values of Table 3 show, k_r increases by a factor of 4, while the enhancement of k_{nr} is tenfold compared to that of CdP^{4-}. This indicates that acceleration of both the radiative and the nonradiative processes are responsible for the change of the fluorescence lifetime and quantum yield, although the reducing effect of k_{nr} is determining. These strong effects can be attributed to both the increased deformation of the porphyrin ring and the additional possibility of nonradiative energy dissipation through the axially coordinated ligand.

The fluorescence spectra of the brominated porphyrins, H_2BrP^{4-}, $CdBrP^{4-}$, and $HOCdBrP^{5-}$ could not be measured in the range of wavelength beyond 900 nm (Fig. 4b) because of the detection limit of our equipment. Even so the emission bands belonging to the $S_1(0,0)$ and partly the $S_1(0,1)$ transitions were recorded and analysed (Table 4). In these cases the resolution by Gaussian curves can compensate, to some extent, the truncation of the spectra. Compared to the emission bands of the corresponding unbrominated species, those of the brominated porphyrins display very large red-shifts (in the range of 2870–3620 cm^{-1}), predominantly due to the strongly distorted structure of the macrocycle. Moreover, the Stokes-shifts in these cases are much higher (about 3.2–5.2 times) than those for the corresponding unbrominated porphyrins, with the values in the range of 1160–1690 cm^{-1}. This phenomenon indicates that, in spite of the considerably nonplanar ground state, much stronger structural distortions occur upon excitation of these species than in the case of the unbrominated compounds. This effect may be attributed to the already strained bond system, the perturbation of which can lead to a structure of a significantly different geometry. The fluorescence quantum yields for H_2BrP^{4-} and $CdBrP^{4-}$ are about one order of magnitude lower than those of the corresponding unbrominated species. One of the most reasonable explanations for the decrease of $\phi(S_1)$ is the heavy-atom effect of the Br substituents, which enhances the rates of radiationless decay in the octabromo compounds due to an increased spin–orbit coupling leading to faster nonradiative intersystem crossing to the triplet states. Such an effect also influences the efficiency of the S_2–S_1 internal conversion (IC). This is manifested in the decrease of the ϕ(IC) values upon bromination. Accordingly, among the MgTPP, ZnTPP, and CdTPP complexes only in the case of the latter one was observed a significant intersystem crossing in the decay of the S_2 state [74]. The decrease of $\phi(S_1)$ upon bromination may also be attributed to the more distorted structure, which results in more intense ring vibrations of the skeleton, being effective in nonradiative energy dissipation. This is in agreement with what was found for three Soret-excited diamagnetic meso-substituted tetraphenylmetalloporphyrins, MgTPP, ZnTPP, and CdTPP, namely that the multiple in-plane C–C and C–N stretches are the vibrational modes that induce the coupling in the S_2–S_1 internal conversion [74]. Instead of the in-plane stretches, in the case of the OOP complexes such as the cadmium(II) porphyrins studied in this work, the out-of-plane stretches become more dominant.

As a consequence of the effects discussed above, the fluorescence lifetimes are at least one order of magnitude shorter for the brominated species. Thus, their subnanosecond values were estimated by the Strickler–Berg equation [73], similar to that of $HOCdP^{5-}$. In the case of $HOCdP^{5-}$ and $HOCdBrP^{5-}$ the values of the corresponding parameters are similar because of the determining role of the axial hydroxo ligand.

In the case of arylated porphyrins the fluorescence from the S_1-state displays a relatively rare peculiarity: its spectrum is antisymmetric with respect to that of the absorption [75]. This phenomenon may be explained by the extension of delocalization by the twisting of aryl substituents to closer to the porphyrin plane, causing an alternating excited state [76] (see also Section 3.4.). For distorted porphyrins such as HgP^{4-} smaller fluorescence vs. absorption spectral antisymmetry was observed [61]. This feature may be attributed to a smaller magnitude of such structural change because in these cases the dihedral angle of the meso-aryl groups is smaller already in the ground-state than in planar porphyrins. Similar spectral property is displayed by CdP^{4-} and, to a smaller extent, by $HOCdP^{5-}$ as well (Figs. 3a and 4a. From Table 3, for H_2P^{4-} $I_{max}(0,1)/I_{max}(0,0)$ is 0.71 in fluorescence while it would be 0.6 if the spectrum were totally antisymmetric to the absorption one from Table 2. The same numbers are 1.00 and 0.43, respectively, for CdP^{4-}, and 0.92 and 0.76 for $HOCdP^{5-}$ from Table 3.) The cadmium(II) ion with a closed-shell [Kr]$5d^{10}$ electron configuration does not luminesce and does not really influence electronically the emission of ligands in its complexes [77]. Hence, probably the steric effect is responsible for the change of S_1-fluorescence in its porphyrin complexes. The values of $I_{max}(0,1)/I_{max}(0,0)$ could not be reliably estimated for the brominated derivatives because of the truncated emission spectra. But theoretical structure calculations clearly indicated that the aryl substituents in the ground state of these compounds are twisted more significantly (i.e., having smaller torsion angle) than in the corresponding unbrominated species (see Section 3.4.).

Table 5
The photochemical quantum yields of the free-base and cadmium(II) porphyrins in air-saturated and deoxygenated solution.[a]

Species	H_2P^{4-}	CdP^{4-}	$HOCdP^{5-}$	H_2BrP^{4-}	$CdBrP^{4-}$	$HOCdBrP^{5-}$
Φ(B)/10^{-5}	0.60	39	730	15.6	16.3	104
% Structural	–	3%	20%	–	79%	23%
Φ(B–Ar)/10^{-5}	0.33	44	610	1.65	8.8	12.3
% Structural	–	5%	15%	–	86%	22%
Φ(Q)/10^{-5}	–	70	114	5.4	23	77
% Structural	–	–	–	–	100%	81%
Φ(Q–Ar)/10^{-5}	–	76	108	1.5	4.4	2.3
% Structural	–	–	–	–	100%	85%

[a] Φ(B) and Φ(Q) are the overall photochemical quantum yields observed in Soret- and Q-band photolysis, and "% structural" denotes the photoinduced structural change (dissociation of the axial hydroxo ligand, or that of the metal center in the case of CdP^{4-}, furthermore the formation of the conjugated, chlorin-like photoproduct) fraction of the overall quantum yield.

3.3. Primary photochemistry

While the normal (in-plane) metalloporphyrins do not undergo efficient photoinduced ligand-to-metal charge-transfer reactions, due to their kinetically stable, planar structure, OOP complexes display a characteristic photoredox chemistry featured by irreversible photodegradation caused by the effective separation of the reduced metal center and the oxidized macrocycle following the LMCT reaction, finally leading to irreversible ring cleavage of the ligand, e.g., the formation of the open-chain dioxo-tetrapyrrol derivatives, bilindions [22,61,70,78,79]. The irradiations were carried out at both the Soret- and the Q-bands, in both aerated and argon-saturated systems. These measurements could also contribute to the investigation of the effects of bromination on the photochemical features of these porphyrins.

The quantum yields for the photochemical reactions of the porphyrins in this work are summarized in Table 5. In accordance with our earlier observations [22,57,58,61], the unbrominated free base does not show any measurable change upon irradiation at the Q-bands, and only very slight degradation at the Soret-band excitation in both air-saturated and deaerated solutions. Photolysis of CdP^{4-} at the Soret-band results in the decrease of the absorption at the characteristic bands, indicating an irreversible degradation of the complex, the quantum yield of which is two orders of magnitude higher than that of the free base in aerated system. This phenomenon clearly indicates that the metal center of relatively large ionic radius promotes the photoinduced LMCT followed by an efficient charge separation, which is characteristic for the OOP complexes. Besides the LMCT process, dissociation of CdP^{4-} (to the free base and the metal center) can also observed, but with a small fraction (less than 5%) of the overall quantum yield. Irradiation of this complex at the Q-bands resulted in exclusively redox degradation, although with higher quantum yield than that observed for Soret-band excitation. This phenomenon suggests that S_2 excited state of CdP^{4-} undergoes more efficient energy dissipation processes than its S_1-excited state does, and following the internal conversion the photoredox process finally originates from this latter one. In the absence of oxygen the overall quantum yields are slightly higher than in aerated solution at both Soret- and Q-band irradiations, indicating that dissolved O_2 does not efficiently react with the excited-state porphyrins in these systems, it may cause only a weak quenching effect. Similar tendencies were observed for the photoinduced behaviour of the corresponding complex of mercury(II) (HgP^{4-}) [61]. It confirms that the size of the metal center is predominantly responsible for these peculiarities of the water-soluble OOP metalloporphyrins.

The most interesting transformation upon irradiation was observed in the case of $HOCdP^{5-}$. Upon excitation at the Soret-band, the decrease of the absorption at 431 nm is accompanied by the appearance of a new band at 421 nm, indicating the formation of CdP^{4-} (Fig. 5a).

According to this spectral change, both degradation of the complex due to irreversible ring-cleavage and dissociation of the axial hydroxo ligand take place. The overall quantum yield for the transformation of $HOCdP^{5-}$ at Soret-band excitation is

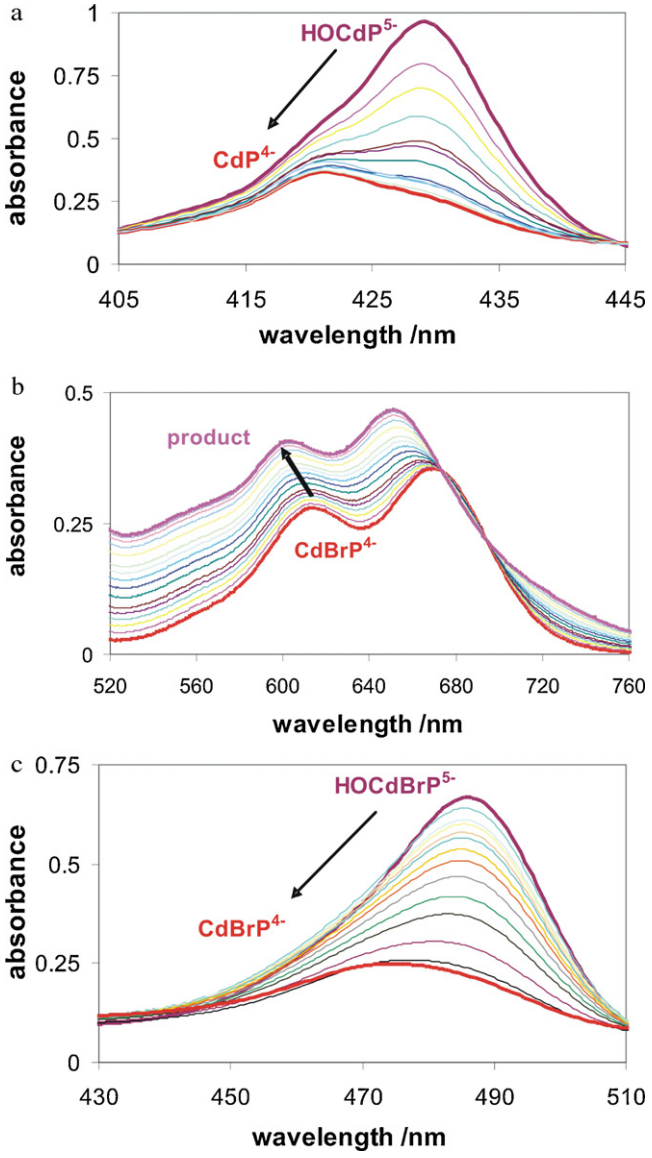

Fig. 5. Spectral changes during the irradiation of $HOCdP^{5-}$ (a), $CdBrP^{4-}$ (b) and $HOCdBrP^{4-}$ (c). (a) $c(H_2P^{4-}) = 2.16 \times 10^{-6}$ M, $c(Cd^{2+}) = 9.99 \times 10^{-6}$ M, $\lambda_{irr} = 429$ nm, $I_0 = 7.98 \times 10^{-6}$ M photon s^{-1}, irradiation time 65 s. (b) $c(H_2BrP^{4-}) = 2.70 \times 10^{-5}$ M, $c(Cd^{2+}) = 3.31 \times 10^{-5}$ M, $\lambda_{irr} = 669$ nm, $I_0 = 3.55 \times 10^{-5}$ M photon s^{-1}, irradiation time 230 min. (c) $c(H_2BrP^{4-}) = 3.14 \times 10^{-6}$ M, $c(Cd^{2+}) = 5.00 \times 10^{-6}$ M, $\lambda_{irr} = 486$ nm, $I_0 = 1.30 \times 10^{-6}$ M photon s^{-1}, irradiation time 64 min.

one order of magnitude higher than that for the reaction of CdP^{4-} in aerated system. This phenomenon may be attributed to the distortion effect of the axial ligand promoting the out-of-plane location of the metal center, and, thus, the more effective separation of the primary products of the photoinduced LMCT reaction. The efficiency for the photoinduced dissociation is 20% of the overall quantum yield (Table 5). The absence of oxygen causes only a slight decrease of both the overall quantum yield and the ratio of the dissociation, indicating that dissolved O_2 does not play any key role in the photochemical reactions of $HOCdP^{5-}$.

Interestingly, irradiation at the Q-bands does not lead to the formation of CdP^{4-}, and the efficiency for the degradation is about 6 times lower than that at Soret-band excitation, but still higher than that for the decomposition of CdP^{4-}. This phenomenon suggests that the energy of the S_1-excited state is not enough for the dissociation of the axial hydroxo ligand, and it is much less effective from the viewpoint of the irreversible LMCT process than the higher (S_2) excited state. The presence of oxygen causes even more slight if any effect in this case too, confirming that oxygen does not take part in these reactions.

Irradiation of the brominated free base at the Soret-band results in an efficient degradation in aerated system, with about 30 times higher quantum yield than that for the unbrominated porphyrin. Removal of oxygen in this case, however, significantly (about one order of magnitude) diminishes the degradation efficiency. This phenomenon implies that the S_2-excited-state free base undergoes an efficient oxidative quenching by dissolved O_2. This oxygen sensitivity may be attributed to the non-bonding electron-pairs on the peripheral bromine atoms, being suitable targets of electrophile attack by oxygen molecules. Excitation at the Q-bands led also to degradation of H_2BrP^{4-}, although with a somewhat lower quantum yield under aerated conditions, but in argon-saturated system the efficiency is close to that observed at the Soret-band irradiation. This suggests that the S_1-excited state is as similarly effective as S_2 in respect of an intramolecular reaction leading to ring cleavage. Such a reaction, which the unbrominated free base does not undergo, may be attributed to the distortion and electron-withdrawing effects of the Br substituents. Deviating from the corresponding unbrominated species, Soret-band irradiation of $CdBrP^{4-}$ results in a less efficient transformation than that observed for CdP^{4-} in aerated solution. The overall quantum yield for the disappearance of the brominated derivative is about the same as that for the degradation of the corresponding free base. However, the decrease of the characteristic absorption of $CdBrP^{4-}$ is accompanied by the appearance of a new species, which still reserved the conjugated bond system, probably a chlorin-like product on the basis of its individual spectrum (Fig. 5b). The ratio of this reaction is rather high (about 80%) within the overall quantum yield. Q-band irradiation of $CdBrP^{4-}$ results in the same type of transformation with the efficiency even higher than that for Soret-band excitation, but the ratio of the formation of conjugated photoproduct is 100%. Deoxygenation, like in the case of the brominated free base, drastically diminishes the quantum yields at both Soret- and Q-band irradiation.

Similarly to the case of $HOCdP^{5-}$, irradiation of the corresponding brominated species, $HOCdBrP^{5-}$ leads also to both dissociation of the axial hydroxo ligand and irreversible ring-cleavage (Fig. 5c). However, the overall quantum yield in this case is about one order of magnitude lower than that for the unbrominated species in aerated system. This is consistent with the tendency observed for the complexes without axial hydroxo ligands. Similarly, the quantum yield at Q-band irradiation is significantly lower than that at Soret-band excitation, and deoxygenation dramatically decreases the efficiency in both cases.

3.4. Electronic structure calculations

The main purpose of our electronic structure calculations was to reveal the geometrical structure of the CdP^{4-}, $HOCdP^{5-}$, $CdBrP^{4-}$, and $HOCdBrP^{5-}$ complexes, as well as the corresponding free-base porphyrins, H_2P^{4-} and H_2BrP^{4-}, and to detect whether there is a correlation between the features of geometry, the electronic spectrum and the photochemical behaviour. Within this investigation, elucidation of the effects of bromination on these properties was especially important. In the calculations, we used a model in which the sulfonato substituents on the peripheral phenyl groups, present in our experiments, were omitted. We expect that influences by the interaction and relative size of the cavity and the metal center (Cd^{2+}), the bromine atoms in β-position, and the axial hydroxo ligand can be correctly described by this model. Perspective representations of the calculated geometries are shown in Fig. 6.

Listed in Table 6 are the most characteristic numerical data corresponding to the calculated structures: parameters related to the location of the metal center, the size of the cavity, and some parameters characterizing the geometrical distortion of the macrocycle for all the six species studied. Besides, the calculated wavelengths at the peaks of the main Soret- and Q-bands are also displayed.

In the upper part of Table 6 are summarized the distances of the atoms from the approximate N–N–N–N plane, more precisely, from the plane that passes through only the diagonally situated N_1 and N_2 and is parallel to the overall plane of the molecule, i.e., the plane perpendicular to the straight line that is the remnant of the C_4 axis of the undistorted porphyrin ring. In the following we shall refer to this plane as "N_1–N_2 plane". In the out-of-plane distorted structures the other two diagonally situated nitrogen atoms (N_3 and N_4) are located below the N_1–N_2 plane, and in free-base porphyrins they hold H atoms which are located above N_1–N_2 plane. The Cd atom can be located between or outside of the two parallel planes passing through the two respective pairs of diagonally located N atoms. The degree of distortion of the porphyrin ring is most straightforwardly characterized by the distance from the N_1–N_2 plane of the α- and, especially, the β-carbon atoms of the ring as well as those of the hydrogen or bromine atoms bound to C_β. The distance corresponding to the O atom and the H bound to it indicates the position of the axial hydroxo ligand.

In the lower part of the table, the distances of the diagonally situated nitrogen atoms are shown, indicating the actual size of the cavity. It is slightly influenced by the interaction with the metal center as it can be seen later. Also the torsion angles are of the phenyl rings relative to the mean plane of the macrocycle are given (defined by the C_α–C_m–C_1–C_2 dihedral angle, where C_1 and C_2 are the corresponding carbon atoms of the phenyl group). In the last two rows are summarized the calculated wavelengths of the main Soret- and Q-bands.

In the case of the unbrominated species, no appreciable distortion of the macrocycle can be observed for H_2P^{4-} and CdP^{4-} (Fig. 6a and b). The data indicate that insertion of the Cd^{2+} ion into the porphyrin does not change the planar structure of the ligand. The metal center is located in the ligand core, between the two nitrogen planes. In the free-base porphyrin the N_1–N_2 distance is shorter than the N_3–N_4 one, due to the presence of the hydrogen atoms on the latter nitrogen atoms. In the CdP^{4-} complex, however, the two diagonal N–N distances are equivalent because the protons originally located on N_3 and N_4 are not present. Besides, the N–N distances are noticeably longer, indicating that the insertion of the Cd^{2+} ion into the coordination cavity pushes the pyrrolic nitrogens apart into an approximately in-plane position. At the same time the N_3 and N_4 atoms are lifted slightly further from the reference plane. Coordination of a hydroxo ligand in the axial position (forming $HOCdP^{5-}$) significantly modifies the structure of the complex (Fig. 6c). It pulls the Cd^{2+} ion out of the ligand center

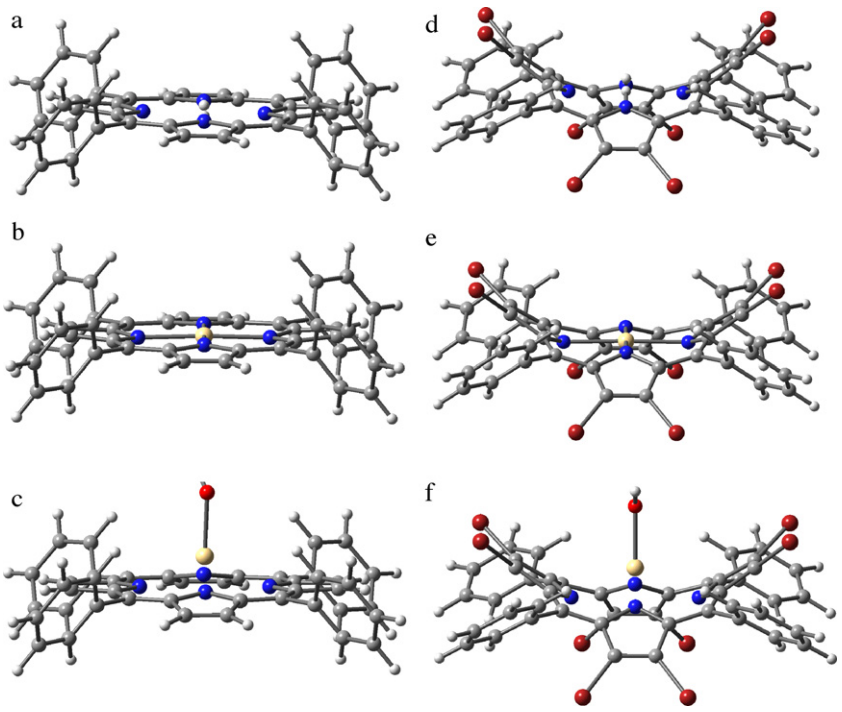

Fig. 6. The structure of H_2P^{4-} (a), CdP^{4-} (b), and $HOCdP^{5-}$ (c), and those of the corresponding octabromo derivatives, H_2BrP^{4-} (d), $CdBrP^{4-}$ (e), and $HOCdBrP^{5-}$ (f) obtained at the B3LYP/LANL2DZ level of theory (the sulfonato substituents are omitted because of their negligible effect on the coordination site).

so that it is located about 100 pm above the plane of the nitrogen atoms. Thus, the N–N distances decrease, becoming slightly different again although not to the extent observed in the free base. The out-of-plane (or sitting-atop) position of the metal center results in a moderate out-of-plane distortion of the porphyrin ring, indicated by the increased distances of the C_α and C_β atoms, as well as that of the H atom on the C_β atoms from the reference plane.

Comparison of the location of the calculated absorption maxima with the experimental results shows a reasonable agreement. Even though the numerical values do not perfectly coincide (but are surprisingly close as compared to the level of approximation used in TD-DFT), the tendencies definitely agree. There is a correlation between the magnitude of distortion of the porphyrin ring and the red shift of the absorption maxima. It should be noted, however, that not only the distortion but also the relative contribution of various molecular orbital-to-molecular orbital transitions (e.g., porphyrin rings vs. phenyl rings) varies along the series of compounds. Accordingly, the increasing twist of the phenyl rings towards the plane of the macrocycle promotes its orbitals to contribute to the conjugated bond system of the porphyrin to a larger extent, resulting in red shifts of the absorption bands [23,76]. The decreasing torsion angles calculated are in good agreement with the increasing batochromic shifts of the unbrominated metalloporphyrins, CdP^{4-} and $HOCdP^{5-}$, at both the Soret- and the Q-bands.

The structural features of the corresponding octabrominated derivatives are significantly different from those of the unbrominated compounds. Already the free base itself (H_2BrP^{4-}, Fig. 6d) is strongly distorted as indicated by the distances of the C_α and, especially, C_β atoms. According to them, the porphyrin ring possesses a saddle shape: the C_α (and C_β) atoms of neighbouring pyrrole groups

Table 6
The calculated structural data of the unbrominated porphyrins (H_2P^{4-}, CdP^{4-}, and $HOCdP^{3-}$) and their octabromo derivatives (H_2BrP^{4-}, $CdBrP^{4-}$, and $HOCdBrP^{3-}$), along with the wavelengths of their main Soret- and Q-bands (see text for details).

Distance/pm	H_2P^{4-}	CdP^{4-}	$HOCdP^{5-}$	H_2BrP^{4-}	$CdBrP^{4-}$	$HOCdBrP^{5-}$
N_1, N_2	0	0	0	0	0	0
Cd, H	2	4	99	41	4	102
N_3	4	9	9	15	8	6
N_4	4	9	12	15	8	7
C_α	1	2	11	54	30	42
C_β	13	10	44	138	106	133
C_m	2	3	9	8	4	3
X = Br, H	23	20	68	252	213	258
O			310			310
H			371			373
d(N_1–N_2)	409	431	422	422	437	431
d(N_3–N_4)	424	431	425	427	431	425
Dihedral angle/°						
Phenyl twisting[a]	65.5	63.8	60.5	55.3	55.5	51.5
Wavelengths/nm						
λ_{max}(B)[b]	367	384	414	433	454	459
λ_{max}(Q)[b]	565	566	652	661 (697)[c]	688	734

[a] C_α–C_m–C_1–C_2.
[b] Average values of B_x and B_y or Q_x and Q_y.
[c] The wavelength of Q_x absorption is given in the parenthesis.

are located alternating above and below the average plane of the nitrogen atoms. The carbon atoms in meso- (or bridge-) position (C_m) are situated in the reference plane, while the phenyl groups connecting to them contribute to the distortion. Of course, the main reason of the distortion is the steric demand of the Br substituents on the C_β atoms. The Br atoms, being much larger than H atoms cannot be accommodated in a plane if there are phenyl rings on the meso carbon atoms. More quantitatively, the distance of the bromine atoms from the reference plane is very large, exceeding 250 pm. The N_3 and N_4 atoms are slightly above this plane, and the H atoms on them are even further above (41 pm). This asymmetric location of the pyrrolic nitrogens makes their accessibility more favourable for the coordinating metal ions due to the increase of the degree of their sp^3 hybridization. Interestingly, the N_1–N_2 and N_3–N_4 distances are not as different as in the case of the unbrominated free base (5 pm vs. 15 pm), because the pyrroles with N_1 and N_2 are also twisted, even if very slightly, around their C_α–C_α axis.

Insertion of the Cd^{2+} ion into the porphyrin considerably modifies the structure of the ligand (Fig. 6e). Similarly to the corresponding unbrominated complex, the metal center is located in the cavity of the macrocycle, pushing the nitrogen atoms apart. Also the N_3 and N_4 atoms approach the reference plane to about the same distance (8–9 pm) as in the unbrominated derivative. In this case, however, the difference between the N_1–N_2 and N_3–N_4 distances remains about the same as in the free base (5–6 pm). The presence of the metal center significantly decreases the saddle distortion of the porphyrin ring partly due to the expansion of the coordination cavity. Both the C_α and C_β atoms and the Br substituents on the latter ones are much closer to the reference plane but the diagonal distances between the pyrrol-nitrogens are longer than in the free base.

Coordination of a hydroxo ligand in the axial position, however, restores the stronger distortion (Fig. 6f). Similarly to the corresponding unbrominated species, the metal center is pulled out of the ligand plane, over 100 pm above it, and the diagonal N–N distances decrease. The nitrogen atoms (N_3 and N_4), however, remain close (or get very slightly closer) to the reference plane (6–7 pm). The deviations of the carbon atoms (C_α and C_β) and the bromine substituents from the ligand plane become similar to those in the free base, indicating a more distorted saddle structure. The stronger distortion together with the electronic effects of the bromine substituents causes significant red shifts of the absorption bands with respect to those of the corresponding unbrominated species. Insertion of the Cd^{2+} ion, however, decreases the distortion, which is manifested in the slight blue-shift of the Q-band compared to that of Q_x-band of the free-base porphyrin, deviating from the tendency observed in the case of the unbrominated species. Axial coordination of the metal, through the increased distortion, results in more pronounced bathochromic shifts of the main absorption bands. Similarly to the case of the unbrominated compounds, the tendency of the wavelengths calculated agrees well with that of the measured ones for the Q-bands, but much less for the Soret-bands. This discrepancy is within the limits of accuracy of the TDDFT method. The calculated twists of the phenyl rings relative to the mean plane of the macrocycle are also in good accordance with the positions of the absorption bands. The ca. 10° decrease of the dihedral angles of the phenyl groups in the brominated species compared to those of the corresponding unbrominated derivates may significantly contribute to the bathochromic shifts of the absorption bands observed upon bromination. Besides, the smaller distorsion angle in $HOCdBrP^{5-}$ than that in $CdBrP^{4-}$ is also in agreement with the red shifts of both the Soret- and the Q-bands. The distorsion angle in $CdBrP^{4-}$ is equal to that in the free base (H_2BrP^{4-}), which is in good correlation with the slight blue shift of the Q-band upon metalation.

4. Conclusion

Both 5,10,15,20-tetrakis(4-sulphonatophenyl)porphyrin and its octabromo derivative readily react with cadmium(II) ions at pH 8, forming metalloporphyrins with axial hydroxo ligand ($HOCdP^{5-}$ and $HOCdBrP^{5-}$). Removal of this axial ligand by either irradiation or acidification leads to the formation of the corresponding complexes, CdP^{5-} and $CdBrP^{5-}$ of less distorted structure. Photolysis of both complexes with HO^- in axial position results in both ligand dissociation and LMCT process followed by irreversible ring cleavage of the macrocycle. The CdP^{5-} and $CdBrP^{5-}$ complexes, however, undergo deviating photochemical reactions. While irradiation of the unbrominated complex leads to the degradation of the porphyrin ring, the brominated derivative is transformed to a new species reserving the conjugated bond system of the macrocyclic ligand. The photochemical reactions of the unbrominated porphyrins are hardly affected by dissolved O_2, whereas those of the brominated derivatives proved to be very oxygen sensitive. The results of the DFT calculations, demonstrating the strong distortion in the brominated porphyrins, are in good correlations with the bathochromic shifts of the absorption and emission bands. These results contribute to the elucidation of the effects caused by the bromination of the water-soluble porphyrins concerning their photophysical and photochemical behaviour. Further studies on the formation kinetics of these complexes and for comparison of the photoinduced properties of other metalloporphyrins and their brominated derivates are in progress.

Acknowledgements

This work was supported by the National Development Agency (TÁMOP 4.2.2.-08/1/2008-0018, Livable environment and healthier people–Bioinnovation and Green Technology research at the University of Pannonia, the project is being co-financed by the European Social Fund with the support of the European Union) and also in the frame of the Hungarian–Croatian Intergovernmental S&T Cooperation Program for 2009–2010 jointly financed by the Hungarian National Office of Research and Technology (OMFB-01247/2009). GL thanks for support by the Hungarian Scientific Research Fund (grant no. OTKA K77938).

References

[1] R.H. Garrett, C.M. Grisham, Biochemistry, Saunders College Publishing, 1999.
[2] C.K. Mathews, K.E. van Holde, K.G. Ahern, Biochemistry, Addison Wesley Longman, San Francisco, 2000.
[3] G.G. Martirosyan, A.S. Azizyan, T.S. Kurtikyan, P.C. Ford, Low temperature NO disproportionation by Mn porphyrin. Spectroscopic characterization of the unstable nitrosyl nitrito complex Mn^{III}(TPP)(NO)(ONO), Chem. Commun. (2004) 1488–1489.
[4] M.D. Lim, I.M. Lorkovic, P.C. Ford, NO and NO_x interactions with model group 8 metalloporphyrins, J. Inorg. Biochem. 99 (2005) 151–165.
[5] G. Knör, A. Strasser, Enhanced photoreactivity of zirconium(IV) and hafnium(IV) porphyrin complexes promoted by water molecules, Inorg. Chem. Commun. 9 (2005) 471–473.
[6] E.B. Fleischer, J.H. Wang, The detection of a type of reaction intermediate in the combination of metal ions with porphyrins, J. Am. Chem. Soc. 82 (1960) 3498–3502.
[7] K.M. Barkigia, J. Fajer, A.D. Adler, G.J.B. Williams, Crystal and molecular structure of (5,10,15,20-tetra-N-propylporphinato)lead(II): a roof porphyrin, Inorg. Chem. 19 (1980) 2057–2061.
[8] J.Y. Tung, J.-H. Chen, Crystal and molecular structure of an eight-coordinate N-methyltetraphenylporphyrin complex: diacetato(N-methyl-meso-tetraphenylporphyrinato)thallium(III), Inorg. Chem. 39 (2000) 2120–2124.
[9] C. Stinson, P. Hambright, The copper-cadmium N-methyltetraphenylporphyrin electrophilic substitution reaction: evidence for a cis attack, J. Am. Chem. Soc. 99 (1977) 2357.
[10] M. Tabata, M. Tanaka, A new method for the determination of the stability constant of metalloporphyrins, use of the catalytic effect of mercury(II) on metalloporphyrin formation, J. Chem. Soc. Chem. Commun. (1985) 42–43.
[11] K.M. Barkigia, M.D. Berber, J. Fajer, C.J. Medforth, M.W. Renner, K.M. Smith, Nonplanar porphyrins. X-ray structures of (2,3,7,8,12,13,17,18-octaethyl- and

-octamethyl-5,10,15,20-tetraphenylporphinato)zinc(II), J. Am. Chem. Soc. 112 (1990) 8851–8857.
[12] L.R. Robinson, P. Hambright, Mercury(II) reactions with water-soluble porphyrins, Inorg. Chem. 31 (1992) 652–656.
[13] M. Tabata, W. Miyata, N. Nahar, Kinetics and mechanism of metal-substitution reaction of homodinuclear mercury(II) porphyrin with zinc(II) with particular reference to a heterodinuclear metalloporphyrin intermediate, Inorg. Chem. 34 (1995) 6492–6496.
[14] M. Inamo, N. Kamiya, Y. Inada, M. Nomura, S. Funahashi, Structural characterization and formation kinetics of sitting-atop (SAT) complexes of some porphyrins with copper(II) ion in aqueous acetonitrile relevant to porphyrin metalation mechanism. Structures of aquacopper(II) and Cu(II)-SAT complexes as determined by EXAFS spectroscopy, Inorg. Chem. 40 (2001) 5636–5644.
[15] D.K. Lavallee, Kinetics and mechanisms of metalloporphyrin reactions, Coord. Chem. Rev. 61 (1985) 55–96.
[16] M. Tabata, M. Tanaka, Porphyrins as reagents for trace-metal analysis, Trends Anal. Chem. 10 (1991) 128–133.
[17] P. Bhyrappa, V. Krishnan, Octabromotetraphenylporphyrin and its metal derivatives: electronic structure and electrochemical properties, Inorg. Chem. 30 (1991) 239–245.
[18] D. Mandon, P. Ochsenbein, J. Fischer, R. Weiss, K. Jayaraj, R.N. Austin, A. Gold, P.S. White, O. Brigaud, P. Battioni, D. Mansuy, β-Pyrrole halogenated porphyrins. Molecular structures of 2,3,7,8,12,13,17,18-Octabromo-5,10,15,20-tetramesityl-porphyrin, nickel(II)-[2,3,7,8,12,13,17,18-octabromo-5,10,15,20-tetramesitylporphyrin] and nickel(II)-[2,3,7,8,12,13,17,18-octabromo-5,10,15,20-tetra(pentafluorophenyl)porphyrin], Inorg. Chem. 31 (1992) 2044–2049.
[19] L.M. Henling, W.P. Schaeffer, J.A. Hodge, M.E. Hughes, H.B. Gray, Copper(II) and nickel(II) octabromo-tetrakis(pentafluorophenyl)porphyrin complexes, Acta Crystallogr. C 49 (1993) 1743–1744.
[20] E.R. Brinbaum, J.A. Hodge, M.W. Grinstaff, W.P. Schaefer, L. Henling, J.A. Labinger, J.E. Bercaw, H.B. Gray, ^{19}F NMR spectra and the structures of halogenated porphyrins, Inorg. Chem. 34 (1995) 3625–3632.
[21] N. Nahar, M. Tabata, Kinetics, Mechanism of the reaction of mercury(II) with a water-soluble octabromoporphyrin, J. Porphyr. Phthalocyan. 2 (1998) 397–403.
[22] O. Horváth, R. Huszánk, Z. Valicsek, G. Lendvay, Photophysics and photochemistry of kinetically labile, water-soluble porphyrin complexes, Coord. Chem. Rev. 250 (2006) 1792–1803.
[23] H. Ryeng, A. Ghosh, Do nonplanar distortions of porphyrins bring about strongly red-shifted electronic spectra? Controversy, consensus, new developments, and relevance to chelatases, J. Am. Chem. Soc. 124 (2002) 8099–8103.
[24] O.A. Golubchikov, S.G. Pukhovskaya, E.M. Kuvshinova, Structures and properties of spatially distorted porphyrins, Russ. Chem. Rev. 74 (2005) 249–264.
[25] M. Sankar, C. Arunkumar, P. Bhyrappa, Unusual solvent dependent electronic absorption spectral properties of nickel(II) and copper(II) perhaloporphyrins, J. Porphyr. Phthalocyan. 8 (2004) 1343–1355.
[26] R.D. Shannon, Revised effective ionic radii and systematic studies of interatomic distances in halides and chalcogenides, Acta Cryst. A32 (1976) 751–767.
[27] M. Tabata, M. Tanaka, Kinetics and mechanism of cadmium(II) ion assisted incorporation of manganese(II) into 5,10,15,20-tetrakis(4-sulphonatophenyl)-porphyrinate(4-), J. Chem. Soc. Dalton Trans. (1983) 1955–1959.
[28] M. Tabata, K. Ozutsumi, Equilibrium, EXAFS studies of mercury(II) porphyrin in aqueous solution, Bull. Chem. Soc. Jpn. 65 (1992) 1438–1444.
[29] M. Tabata, J. Nishimoto, A. Ogata, T. Kusano, N. Nahar, Metalation of water-soluble octabromoporphyrin with lithium(I), cadmium(II) and mercury(II), Bull. Chem. Soc. Jpn. 69 (1996) 673–677.
[30] M. Inamo, A. Tomita, Y. Inagaki, N. Asano, K. Suenaga, M. Tabata, S. Funahashi, Equilibria, kinetics and mechanism of complexation of 5,10,15,20-tetrakis(4-sulphonatophenyl)porphyrin and its N-methylated derivate with cadmium(II) and zinc ions in aqueous solution at various temperatures and pressures. Effects of metal ion size and porphyrin ring deformation on metal ion incorporation, Inorg. Chim. Acta 256 (1997) 77–85.
[31] G.P. Chacko, P. Hambright, Acid- anion- and base-catalyzed solvolysis reactions of a water soluble bismuth(III) porphyrin, Inorg. Chem. 33 (1994) 5595–5597.
[32] K. Kilian, K. Pyrzynska, Spectrophotometric study of Cd(II), Pb(II), Hg(II) and Zn(II) complexes with 5,10,15,20-tetrakis(4-carboxylphenyl)porphyrin, Talanta 60 (2003) 669–678.
[33] S. Igarashi, T. Aihara, T. Yotsuyanagi, Flow injection spectrophotometric determination of ng ml-levels of cobalt(II) using the photochemical decomposition of a cadmium(II)-water-soluble porphyrin complex, Anal. Chim. Acta 323 (1996) 63–67.
[34] J.N. Demas, G.A. Crosby, The measurement of photoluminescence quantum yields, J. Phys. Chem. 75 (1971) 991–1024.
[35] J. Van Houten, R.J. Watts, Temperature-dependence of photophysical and photochemical properties of tris(2,2′-bipyridyl)ruthenium(II) ion in aqueous-solution, J. Am. Chem. Soc. 98 (1976) 4853–4858.
[36] K.L. Stevenson, R.M. Berger, M.M. Grush, J.C. Stayanoff, A. Horváth, O. Horváth, Photoinduced electron transfer and luminescence in aqueous bromocuprate(I) complexes, J. Photochem. Photobiol. A 60 (1991) 215–227.
[37] J.N. Demas, Excited State Lifetime Measurements, Academic Press, Inc., New York, 1983.
[38] J.F. Rabek, Experimental Methods in Photochemistry and Photophysics, Wiley-Interscience Publication, John Wiley & Sons Ltd., New York, 1982.
[39] S.L. Murov, Handbook of Photochemistry, Marcel Dekker, New York, 1973.
[40] A.D. Kirk, C. Namasivayam, Errors in ferrioxalate actinometry, Anal. Chem. 55 (1983) 2428–2429.
[41] A.D. Becke, A new mixing of Hartree–Fock and local density–functional theories, J. Chem. Phys. 98 (1993) 1372–1377.
[42] A.D. Becke, Density–functional thermochemistry. 3. The role of exact exchange, J. Chem. Phys. 98 (1993) 5648–5652.
[43] C. Lee, W. Yang, R.G. Parr, Development of the Colle–Salvetti correlation-energy formula into a functional of the electron density, Phys. Rev. B37 (1988) 785–789.
[44] P.J. Hay, W.R. Wadt, Abinitio effective core potentials for molecular calculations – potentials for transition-metal atoms Sc to Hg, J. Chem. Phys. 82 (1985) 270–283.
[45] W.R. Wadt, P.J. Hay, Abinitio effective core potentials for molecular calculations – potentials for main group elements Na to Bi, J. Chem. Phys. 82 (1985) 284–298.
[46] P.J. Hay, W.R. Wadt, Abinitio effective core potentials for molecular calculations – potentials for K to Au including the outermost core orbitals, J. Chem. Phys. 82 (1985) 299–310.
[47] C.E. Check, T.O. Faust, J.M. Bailey, B.J. Wright, T.M. Gilbert, L.S. Sunderlin, Addition of polarization and diffuse functions to the LANL2DZ basis set for p-block elements, J. Phys. Chem. A 105 (2001) 8111–8116.
[48] Gaussian 03, Revision E.01, M. J. Frisch, G. W. Trucks, H. B. Schlegel, G. E. Scuseria, M. A. Robb, J. R. Cheeseman, J. A. Montgomery, Jr., T. Vreven, K. N. Kudin, J. C. Burant, J. M. Millam, S. S. Iyengar, J. Tomasi, V. Barone, B. Mennucci, M. Cossi, G. Scalmani, N. Rega, G. A. Petersson, H. Nakatsuji, M. Hada, M. Ehara, K. Toyota, R. Fukuda, J. Hasegawa, M. Ishida, T. Nakajima, Y. Honda, O. Kitao, H. Nakai, M. Klene, X. Li, J. E. Knox, H. P. Hratchian, J. B. Cross, V. Bakken, C. Adamo, J. Jaramillo, R. Gomperts, R. E. Stratmann, O. Yazyev, A. J. Austin, R. Cammi, C. Pomelli, J. W. Ochterski, P. Y. Ayala, K. Morokuma, G. A. Voth, P. Salvador, J. J. Dannenberg, V. G. Zakrzewski, S. Dapprich, A. D. Daniels, M. C. Strain, O. Farkas, D. K. Malick, A. D. Rabuck, K. Raghavachari, J. B. Foresman, J. V. Ortiz, Q. Cui, A. G. Baboul, S. Clifford, J. Cioslowski, B. B. Stefanov, G. Liu, A. Liashenko, P. Piskorz, I. Komaromi, R. L. Martin, D. J. Fox, T. Keith, M. A. Al-Laham, C. Y. Peng, A. Nanayakkara, M. Challacombe, P. M. W. Gill, B. Johnson, W. Chen, M. W. Wong, C. Gonzalez, J. A. Pople, Gaussian, Inc., Wallingford CT, 2004.
[49] https://bse.pnl.gov/bse/portal.
[50] K.L. Schuchardt, B.T. Didier, T. Elsethagen, L. Sun, V. Gurumoorthi, J. Chase, J. Li, T.L. Windus, Basis set exchange: a community database for computational science, Chem. Inf. Model. 47 (2007) 1045–1052.
[51] A. Harriman, M.C. Richoux, P. Neta, Redox chemistry of metalloporphyrins in aqueous solution, J. Phys. Chem. 87 (1983) 4957–4965.
[52] K. Kalyanasundaram, Photochemistry of Polypyridine and Porphyrin Complexes, Academic Press, New York, 1992.
[53] K. Kalyanasundaram, M. Neumann-Spallart, Photophysical and redox properties of water-soluble porphyrins in aqueous media, J. Phys. Chem. 86 (1982) 5163.
[54] J.R. Platt, Classification and assignments of ultraviolet spectra of conjugated organic molecules, J. Opt. Soc. Am. 43 (1953) 252–256.
[55] M. Gouterman, Study of the effects of substitution on the absorption spectra of porphyrin, J. Chem. Phys. 30 (1959) 1139–1161.
[56] M. Gouterman, G.H. Wagniére, L.C. Snyder, Spectra of porphyrins: part II. Four orbital model, J. Mol. Spectrosc. 11 (1963) 108–127.
[57] O. Horváth, Z. Valicsek, A. Vogler, Unique photoreactivity of mercury(II) 5,10,15,20-tetrakis(4-sulfonatophenyl)porphyrin, Inorg. Chem. Commun. 7 (2004) 854–857.
[58] Z. Valicsek, O. Horváth, K.L. Stevenson, Photophysics and photochemistry of water-soluble, sitting-atop bis-thallium(I) 5,10,15,20-tetrakis(4-sulfonatophenyl)porphyrin, Photochem. Photobiol. Sci. 3 (2004) 669–673.
[59] R. Huszánk, O. Horváth, A heme-like, water-soluble iron(II) porphyrin: thermal and photoinduced properties, evidences for sitting-atop structure, Chem. Commun. (2005) 224–226.
[60] Z. Valicsek, O. Horváth, Formation, photophysics and photochemistry of thallium(III) 5,10,15,20-tetrakis(4-sulphonatophenyl)porphyrin; new supports of typical sitting-atop features, J. Photochem. Photobiol. A 186 (2007) 1–7.
[61] Z. Valicsek, G. Lendvay, O. Horváth, Equilibrium, photophysical, photochemical and quantum chemical examination of anionic mercury(II) mono- and bisporphyrins, J. Phys. Chem. B 112 (2008) 14509–14524.
[62] J.A. Shelnutt, X.-Z. Song, J.-G. Ma, S.-L. Jia, W. Jentzen, C.J. Medforth, Nonplanar porphyrins and their significance in proteins, Chem. Soc. Rev. 27 (1998) 31–41.
[63] J.A. Shelnutt, Normal-coordinate structural decomposition and the vibronic spectra of porphyrins, J. Porphyr. Phthalocyan. 5 (2001) 300–311.
[64] F. D'Souza, A. Villard, E. Van Caemelbecke, M. Franzen, T. Boschi, P. Tagliatesta, K.M. Kadish, Electrochemical and spectroelectrochemical behavior of cobalt(III), cobalt(II), and cobalt(I) complexes of meso-tetraphenylporphyrinate bearing bromides on the β-pyrrole positions, Inorg. Chem. 32 (1993) 4042–4048.
[65] M. Gouterman, in: D. Dolphin (Ed.), Porphyris, 111, Academic Press, New York, 1978, p. 79.
[66] Z. Oua, J. Shaoa, F. D'Souza, P. Tagliatesta, K.M. Kadish, β-Pyrrole brominated meso-tetraphenylporphyrins: synthesis, spectral and electrochemical properties, J. Porphyr. Phthalocyan. 8 (2004) 201–214.
[67] P. Seybold, M. Gouterman, Porphyrins: XIII: fluorescence spectra and quantum yields, J. Mol. Spectrosc. 31 (1969) 13.
[68] J.R. Darwent, P. Douglas, A. Harriman, G. Porter, M.-C. Richoux, Metal phthalocyanines and porphyrins as photosensitizers for reduction of water to hydrogen, Coord. Chem. Rev. 44 (1982) 83–126.
[69] J.S. Baskin, H.Z. Yu, A.H. Zewail, Ultrafast dynamics of porphyrins in the condensed phase: I. Free base tetraphenylporphyrin, J. Phys. Chem. A 106 (2002) 9837–9844.

[70] R. Huszánk, G. Lendvay, O. Horváth, Air stable, heme-like water-soluble iron(II) porphyrin: in situ preparation and characterization, J. Bioinorg. Chem. 12 (2007) 681–690.
[71] A. Harriman, Luminescence of porphyrins and metalloporphyrins. Part 1. – Zinc(II), nickel(II) and manganese(II) porphyrins, J. Chem. Soc. Faraday Trans. I 76 (1980) 1978–1985.
[72] N. Kobayashi, Theoretical interpretation of spectroscopic data, J. Porphyr. Phthalocyan. 4 (2000) 377–379.
[73] S.J. Strickler, R.A. Berg, Relationship between absorption intensity and fluorescence lifetime of molecules, J. Chem. Phys. 37 (1962) 814–822.
[74] U. Tripathy, D. Kowalska, X. Liu, S. Velate, R.P. Steer, Photophysics of Soret-excited tetrapyrroles in solution. I. Metalloporphyrins: MgTPP, ZnTPP, and CdTPP, J. Phys. Chem. A 112 (2008) 5824–5833.
[75] M. Gouterman, L. Stryer, Fluorescence polarization of some porphyrins, J. Chem. Phys. 37 (1962) 2260–2266.
[76] H.N. Fonda, J.V. Gilbert, R.A. Cormier, J.R. Sprague, K. Kamioka, J.S. Connolly, Spectroscopic, photophysical, and redox properties of some meso-substituted free-base porphyrins, J. Phys. Chem. 97 (1993) 7024–7033.
[77] H. Kunkely, O. Horváth, A. Vogler, Photophysics and photochemistry of mercury complexes, Coord. Chem. Rev. 159 (1997) 85–93.
[78] B. Evans, K.M. Smith, J.A.S. Cavaleiro, Bile pigment studies. Part 4. Some novel reactoins of metallo-porphyrins with thallium(III) and cerium(IV) salts. Ring cleavage of meso-tetraphenylporphyrin, J.C.S. Perkin Trans. I (1978) 768–773.
[79] K.M. Smith, S.B. Brown, R.F. Troxler, J.J. Lai, Mechanism of photo-oxygenation of meso-tetraphenylporphyrin metal complexes, Tetrahedron Lett. 21 (1980) 2763–2766.